JOURNAL OF MATERIALS SCIENCE 33 (1998) 3953–3963

A numerical analysis of failure characteristics of ductile layers in laminated composites

S. B. BINER
Ames Laboratory, Iowa State University, Ames, IA 50011, USA
E-mail: biner@ameslab.gov

In this study, the failure of the ductile layers from collinear, multiple and delaminating cracks that occur in laminated composite systems was studied using a constitutive relationship that accounts for strength degradation resulting from the nucleation and growth of voids. The results indicate that, in laminated composites, void nucleation and growth ahead of the cracks occur at a much faster rate because of evolution of much higher stress values in the interface region. Except for short crack extensions, collinear and multiple cracks develop crack resistance curves similar to that seen for a crack in the ductile layer material as a homogenous isotropic cases. For delaminating crack cases, the fracture behaviour is strongly influenced by the delamination length. The resistance of the ductile layers to crack extension can be significantly reduced by short delamination lengths; however, for large delamination lengths the resistance to crack extension becomes greater than that seen for the ductile material. The results also show that, if the crack tip is at the interface, similar maximum stress values develop in the ductile layers as in the fracture test of the same ductile material, suggesting that ductile–brittle fracture transition behaviour of the ductile layers is dependent upon the extent of the cracks in the brittle layers and fracture characteristics of the brittle layers.

1. Introduction

Laminated composites containing ductile layers are currently under development not only to improve the fracture toughness of inherently brittle intermetallics and ceramics [1–9], but also to increase the relatively low fracture toughness of metal matrix composite systems [10, 11]. Recent reviews treating the contribution of the ductile phase to the composite toughening have indicated that this contribution depends on the strength, volume fraction and failure characteristics of the ductile reinforcing phase. It is also apparent that the failure of the ductile layers is strongly affected by the degree of the constraint that is largely controlled by the interfacial behaviour of the layers [12–14]. These factors in varying degrees have been incorporated into models ranging from very simple [12] to more elaborate crack bridging equations [15–17] to describe the toughening behaviour of the brittle layers. The changes in the fracture mode of the ductile layers from ductile fracture associated with the nucleation and growth of voids to more brittle cleavage or intergranular fracture have also been observed in many of the high-temperature composite systems consisting of body-centred cubic (b.c.c) ductile reinforcements currently under investigation [1–9].

As schematically illustrated in Fig. 1, several failure modes of the brittle layers such as only the formation of collinear cracks, with multiple cracking and with delamination in various lengths are usually seen in most of the experimental studies [1–11]. In this study, the growth of such cracks into the ductile layers is studied by using a constitutive relation that accounts for strength degradation resulting from the nucleation and growth of microvoids in the ductile layers. The results obtained for the laminated composite cases are compared with the growth behaviour of the cracks in the same ductile material as a homogenous isotropic case.

2. Numerical analysis

The basis for the constitutive model for the ductile layers is a flow potential introduced by Gurson [18, 19], in which voids are represented in terms of a single internal variable, f, the void volume fraction:

$$\phi = \frac{\sigma_e^2}{\sigma_m^2} + 2f^* q_1 \cosh\left(\frac{q_2 \sigma_h}{2\sigma}\right) - 1 - q_1^2 f^{*2} = 0 \quad (1)$$

where

$$\sigma_e = \tfrac{3}{2}\sigma' : \sigma', \quad \sigma_h = I : \sigma, \quad \sigma' = \sigma - \tfrac{1}{3}\sigma_h I \quad (2)$$

and σ_m is the flow strength of the ductile layer. The parameters q_1 and q_2 were introduced by Tvergaard [20, 21] in order to provide a better relationship between unit-cell analysis and Equation 1; the case $q_1 = q_2 = 1$ corresponds to Gurson's original formulation. The function f^* was proposed by Tvergaard

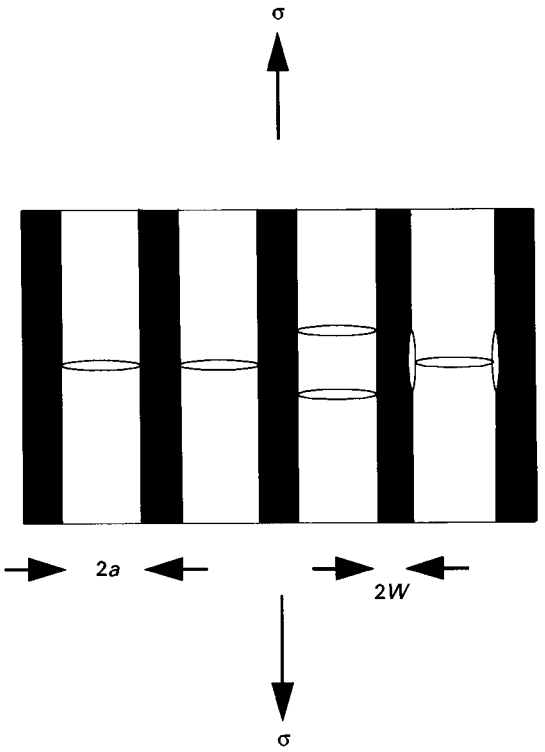

Figure 1 Schematic representation of the crack cases investigated in this study and generally observed in the laminated composites. The dark regions represent the ductile layers.

and Needleman [22] to account for the effect of rapid void coalescence at failure. Initially $f^* = f$ but, at some critical void fraction, f_c, the dependence of f^* and f is changed. This function is expressed by

$$f^* = \begin{cases} f, & f \leqslant f_c \\ f_c + \dfrac{f_u^* - f_c}{f_f - f_c}\,(f - f_c), & f \geqslant f_c \end{cases} \quad (3)$$

The constant, f_u^*, is the value of f^* at zero stress in Equation 1 (i.e., $f_u^* = 1/q_1$) and f_f is the void volume fraction at fracture. As $f \to f_f$, $f^* \to f_u^*$ and the material loses all stress-carrying capacity.

The increase in void volume fraction, f, arises from the growth of existing voids and from the nucleation of new voids. Thus

$$\dot{f} = (\dot{f})_{\text{growth}} + (\dot{f})_{\text{nucleation}} \quad (4)$$

The growth rate is related to the macroscopic dilation rate by

$$(\dot{f})_{\text{growth}} = (1 - f)\delta^{ij}\dot{\eta}_{ij}^{p} \quad (5)$$

where $\dot{\eta}_{ij}^{p}$ is the plastic part of the deformation.

The increase in the volume fraction due to the nucleation process is assumed to occur with strain-controlled nucleation and to follow a normal distribution as suggested by Chu and Needleman [23]:

$$(\dot{f})_{\text{nucleation}} = \left\{ \frac{f_N}{s_N(2\pi)^{1/2}} \exp\left[-\frac{1}{2}\left(\frac{\varepsilon^p - \varepsilon_N}{s_N} \right)^2 \right] \right\} \dot{\varepsilon}^p. \quad (6)$$

where f_N is the volume fraction of void nucleating particles, ε_N is the mean strain for nucleation, ε^p is the current value of effective plastic strain and s_N is the corresponding standard deviation.

In the present investigation a rate-sensitive version of Gurson's model was employed. In the ductile layers, the effective plastic strain rate $\dot{\varepsilon}^p$ is represented by the power-law relation

$$\dot{\varepsilon}^p = \dot{\varepsilon}_0 \left[\frac{\sigma_m}{g(\varepsilon^p)} \right]^{1/m}. \quad (7)$$

where m is the strain rate sensitivity exponent, $\dot{\varepsilon}_0$ is a reference strain rate and ε^p is the current value of the effective plastic strain representing the actual microscopic strain state. The function $g(\varepsilon^p)$ represents the effective tensile flow stress in a tensile test carried out at strain rate that is equal to reference strain rate, $\dot{\varepsilon}_0$. For a power-hardening matric material the function $g(\varepsilon^p)$ is taken to be

$$g(\varepsilon^p) = \sigma_{ys}\left(\frac{E\varepsilon^p}{\sigma_{ys}} + 1 \right)^n, \quad g(0) = \sigma_0. \quad (8)$$

with strain-hardening exponent, n, Young's modulus, E, and reference stress, σ_{ys}. The material parameters for the ductile layer appearing in Equations 7 and 8 were chosen as $E = 500\sigma_{ys}$, u = 0.3, $n = 0.1$, $m = 0.01$ and the reference strain rate, $\dot{\varepsilon}_0 = 2 \times 10^{-3}$. The parameters appearing in Equation 6 for void nucleation were taken as $f_N = 0.04$, $s_N = 0.1$ and $\varepsilon_N = 0.3$. For accelerated void growth, the parameters appearing in Equation 3 were chosen as $f_f = 0.25$, $f_c = 0.10$ and $f_u^* = 1/1.25$. Also, $q_1 = 1.25$ and $q_2 = q_1^2$ were selected for Equation 1. In analysis, the behaviour of the crack-containing brittle layers is assumed to be elastic. The thickness ratio, (W/a), of the ductile layers to the brittle layers was 0.2 (Fig. 1). Young's modulus for the brittle layers was 1.5 times Young's modulus for the ductile layers, and both layers had the same Poission's ratio.

The cases summarized in Fig. 1 were analysed in the plane-strain condition. For the collinear cracks and interface separation cases, because of the symmetry, only one quarter of the geometry is modelled with four-node isoparametric elements as shown in Figs. 2a, d and e. In the case of multiple cracking, half the geometry modelled with the finite-element method (FEM) mesh is shown in Fig. 2c. In all cases, it is assumed that the initial crack tip is located at the interface between the ductile and brittle layers. The crack tip is modelled with a hole having a radius of 10^{-4} of the crack length as shown in Fig. 2b. The smallest element size around the crack tip region was 1.8×10^{-4} of the crack length; to accommodate this large difference in element size and to preserve the aspect ratio of the elements in the finite element discretization the elements were scaled exponentially to the crack tip. Since during the analysis the crack extension behaviour in the ductile layer will be studied, the size of the elements near the crack tip region was kept the same in all cases (Fig. 2a–e). The crack extension is implemented by the element vanishing technique [24]. When the failure condition is met

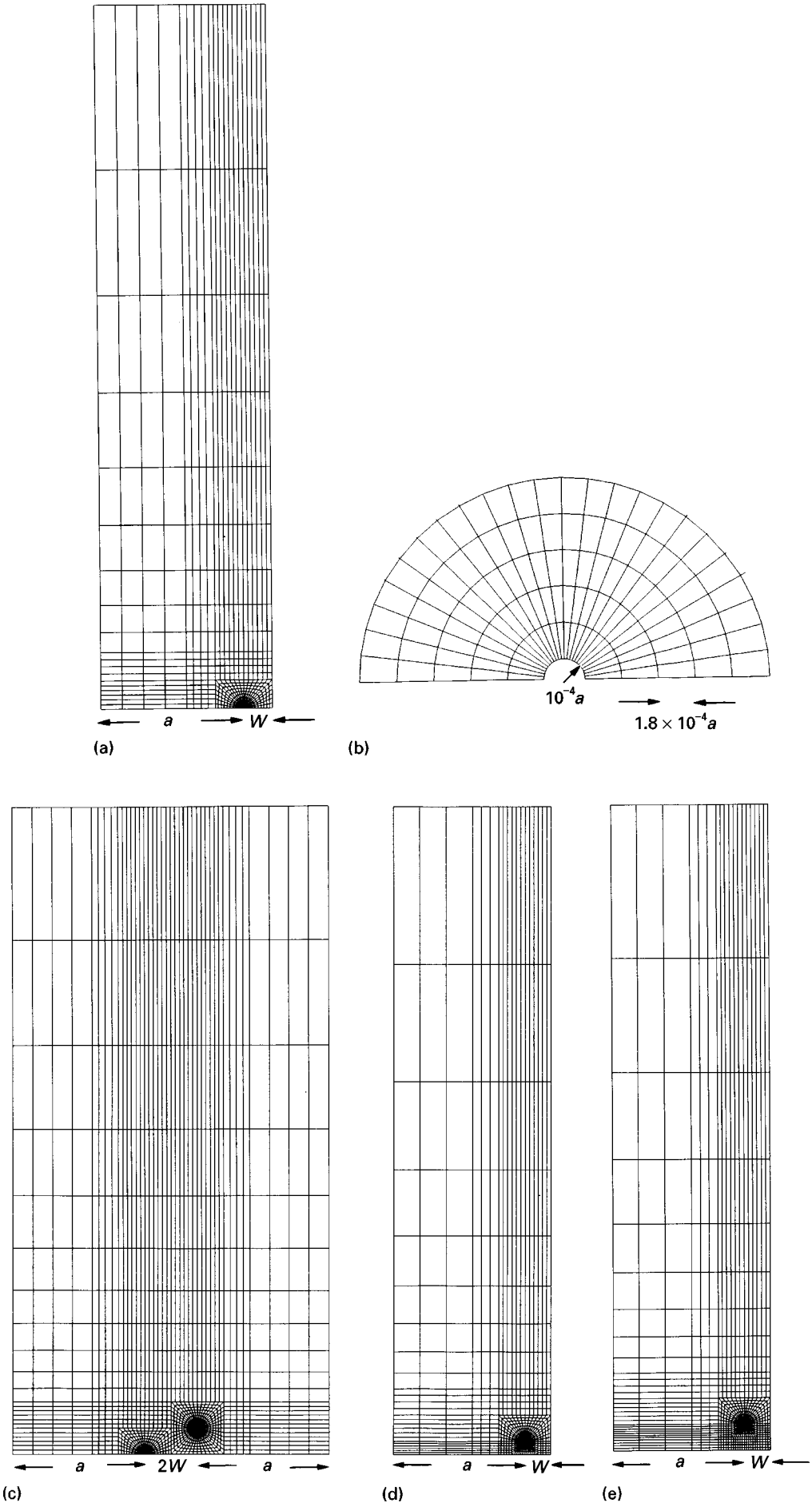

Figure 2 The FEM meshes used in the analysis: (a) for collinear cracks, (b) the details of the crack tip region in all cases; (c) for multiple cracks; (d) for crack having delamination with 0.1 times the original crack length; (e) for crack having delamination with 0.2 times the original crack length.

at all integration points, i.e., $f \geqslant f_f$ that element no longer contributes to the virtual work. To avoid numerical instabilities, the nodal forces arising from the remaining stresses in failed elements are redistributed in several iterations. For all cases, the variation in the void volume fraction ahead of the crack tip is monitored at the third ring elements shown in Fig. 2b. During the analysis the axial displacement rate was equal to the reference strain rate and resulting load values were calculated from the reaction forces. At certain intervals J-integral values were also calculated using

$$J = \int_{\Gamma} \left[\left(\frac{n}{n+1} \sigma_{ij}\varepsilon_{ij} - \sigma_{11}\frac{\partial u_{11}}{\partial x_1} - \sigma_{12}\frac{\partial u_{22}}{\partial x_1} \right) \mathrm{d}x_2 + \left(\sigma_{12}\frac{\partial u_{11}}{\partial x_1} + \sigma_{22}\frac{\partial u_{22}}{\partial x_1} \right) \mathrm{d}x_1 \right]. \quad (9)$$

The area or domain integral procedure outlined in [25] is utilized in the extraction of the J-integral values from the FEM solution. In laminated composites obviously the evaluated J-integral values will depend upon the contour path. To avoid this difficulty, in this study the contour path is chosen to follow the outer most elements seen in Fig. 2 which includes both the elastic and the ductile layers.

3. Results

First, the fracture behaviour of the ductile layer material as a homogeneous isotropic case was elucidated. In order to approximate the stress state in the ductile layers in the laminated composite form, this analysis was carried out using the mesh shown in Fig. 2a as deeply cracked double-edge-notched (DEN) fracture specimen geometry by appropriately choosing the boundary conditions. The resulting load–load-line displacement curve for this case is shown in Fig. 3. The first crack extension from the initial crack occurred in the linear region of the load–load-line displacement curve. Later, because of the spread of the plastic zone to almost the entire uncracked ligament, the crack extension resulting from nucleation and growth of the voids continued in the non-linear regime. As can be seen from Fig. 3, the analysis was carried out well beyond the maximum load. Since the size of the elements increases away from the original crack tip (Fig. 2), the observed step-like behaviour in the load–load-line displacement curve is associated with the failure of the large elements away from the region near the crack tip which required some strain accumulation to meet the failure condition at all integration points. Therefore, it was critical to model the crack tip region with the same element distribution in all cases as described earlier. The evolution of the maximum void volume fraction at the third ring elements (Fig. 2b) with increasing axial displacement is summarized in Fig. 4. As has been well established in the literature, the exponential increase in the void volume fraction ahead of the crack tip with increasing deformation was observed, as can be seen in Fig. 4.

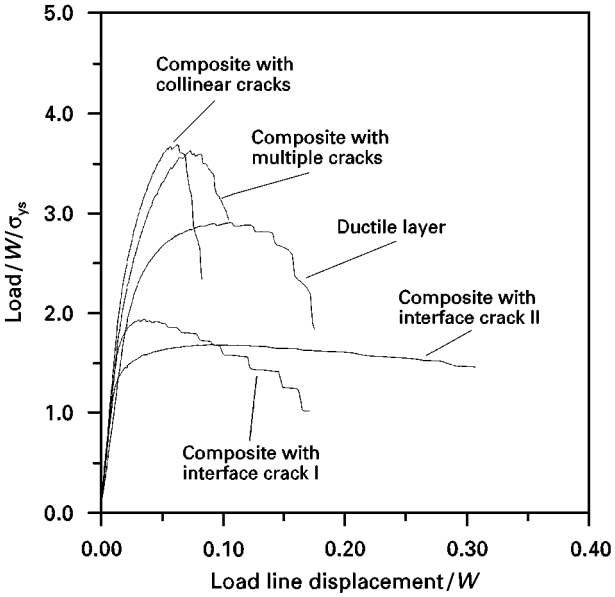

Figure 3 Load–load-line displacement responses of the composites having collinear, multiple and delaminating cracks.

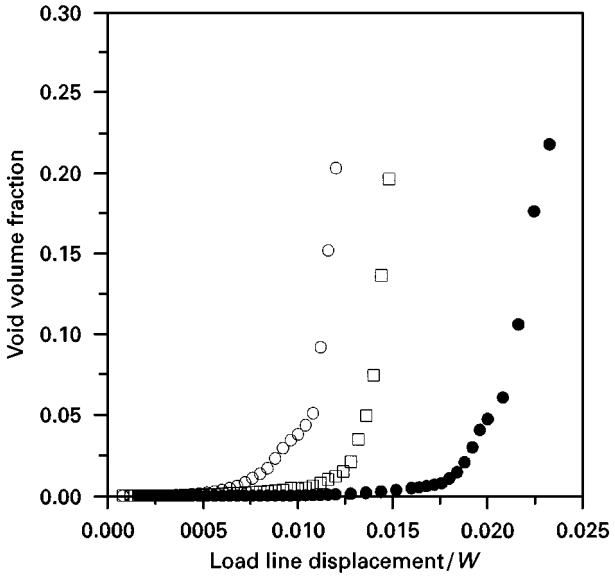

Figure 4 Evolution of the void volume fractions ahead of the collinear (○) and multiple cracks (□) in the laminated composite and comparison with that seen for the crack in the ductile layer (●) as a homogenous isotropic case. The normalized distance, x/W to the crack tip is 2.3×10^{-3}.

In the next two simulations the extension of the collinear cracks and multiple cracks into the ductile layers in the laminated composites were analysed using the meshes shown in Fig. 2a and c, respectively. The resulting load–load-line displacement curves for these cases are also given in Fig. 3. When comparison was made with the previous case, an increase in the overall stiffness at the linear regions of the curves for the laminated composites, owing to the larger Young's modulus of the brittle layers, can be seen in Fig. 3. For these cases, as in the fracture of the ductile material as a homogeneous isotropic case, the first crack extensions also occurred in the linear region. However, for both cases the resulting peak loads were much higher and were achieved at much lower axial displacement

values than seen for the fracture of the ductile layer in DEN specimen having an identical crack length. For both cases, the fracture behaviour was very unstable after the peak loads and very fast reductions occurred in the load-carrying capacity of the uncracked ligaments. Although, in the multiple-cracking case, slightly larger axial displacement was required to achieve crack extensions similar to those occurring in the collinear crack case, the resulting peak load values and the overall responses were similar. The evolution of the maximum void volume fractions at the third ring elements for these cases are also shown in Fig. 4. As can be seen, for the collinear cracks the damage accumulation in the ductile layer occurred at a much faster rate. The axial displacement required for the crack extension from the third row elements was less than half of that required for the fracture of the ductile layer as a homogenous isotropic material. The increase in the void volume fraction in the ductile layer was slower for the multiple crack case owing to the slight loss of stress triaxiality, as will be discussed later; nevertheless for this case the crack tip ductility was still much lower than that seen for the crack as a homogeneous isotropic case.

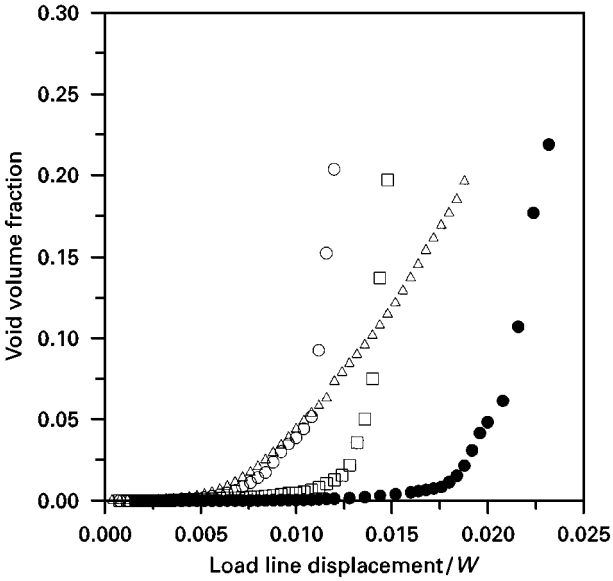

Figure 5 Evolution of the void volume fractions ahead of the delaminating cracks in the laminated composite. (○), composite with collinear cracks; (□), composite with interface crack I; (△), composite with interface crack II; (●) ductile layer. The normalized distance, (x/W) to the crack tip is 2.3×10^{-3}.

In the next two simulations the role of the interface debonding behaviour, as schematically shown in Fig. 1, in the failure behaviour of the ductile layers was investigated. In these analyses, the interface separation distance from the original crack tip were 0.1 and 0.2 times the original crack length and simulated by using the meshes shown in Fig. 2d and e which are designated interface crack I and crack interface II, respectively. In these simulations, it is also assumed that no further debonding at the interface will take place during the fracture process. The resulting load–load-line displacement curves for these cases are also given in Fig. 3. As can be seen from the figure, by introduction of the delamination to the interface, the resulting peak load values were much lower than the composites having only collinear or multiple cracks and this reduction became larger with increasing delamination length. For both delamination cases, the resulting peak loads were even much smaller than that observed during the fracture of the ductile layer as a homogeneous isotropic case. However, as can be seen from Fig. 3, the load–load-line displacement response changes significantly with delamination length. For small delamination length (interface crack I), there was almost no stable crack extension after the peak load; on the other hand, in the case of larger delamination length (interface crack II) the fracture was very stable and it required even larger axial displacements than seen during the fracture process of the ductile layer as a homogeneous isotropic case. The variation in the void volume fractions for these cases, at the same distance ahead of the crack tip as in previous cases, are summarized in Fig. 5. As can be seen from the figure for the composite having a small delamination length, the axial displacement required for the crack extension from the third ring elements is slightly larger than for the composite having only collinear cracks. The axial displacement required for failure to occur at the same location ahead of the crack tip increases with increasing delamination length and approaches that seen for the crack in the ductile layer as a homogeneous isotropic case. In addition, for the larger delamination case, the rate of increase in the volume fraction was much slower than for the other crack cases investigated for the laminated composite.

The displacement fields near the crack tip and the crack extensions at the final load levels for all the cases investigated are shown in Fig. 6. As can be seen from the figure, the directions of the crack extension in the homogeneous crack case and collinear cracks in the laminated composite were very similar. For the multiple-cracking case, similar crack extensions took place from both crack tips (Fig. 6c). In the case of the cracks having an interface separation (Fig. 6d and e), the crack extension significantly deviated from the direction of the delaminated crack tip and the growth directions were towards the centre of the unracked ligament of the ductile layer in the form of a very pronounced shear mode. Also from the figure, for about the same amount of crack extensions a significant increase in the necking of the uncracked ligament together with the larger crack openings with increasing delamination length can easily be seen. Complementary to Fig. 6, the development of equivalent plastic strains at the final load levels is given in Fig. 7. In both laminated composites having collinear and multiple cracks a large extension of the plastic zone along the interface region can be distinguished (Fig. 7b and c). For collinear cracks in the laminated composite, except in the interface region, the extent of deformation in the ligament is not as widespread as that seen for the homogeneous case (Fig. 7b). In the case of multiple cracks, the deformation is largely confined to the crack tip regions owing to significant reductions in the stress values in the regions between the multiple parallel cracks. The evolution of the

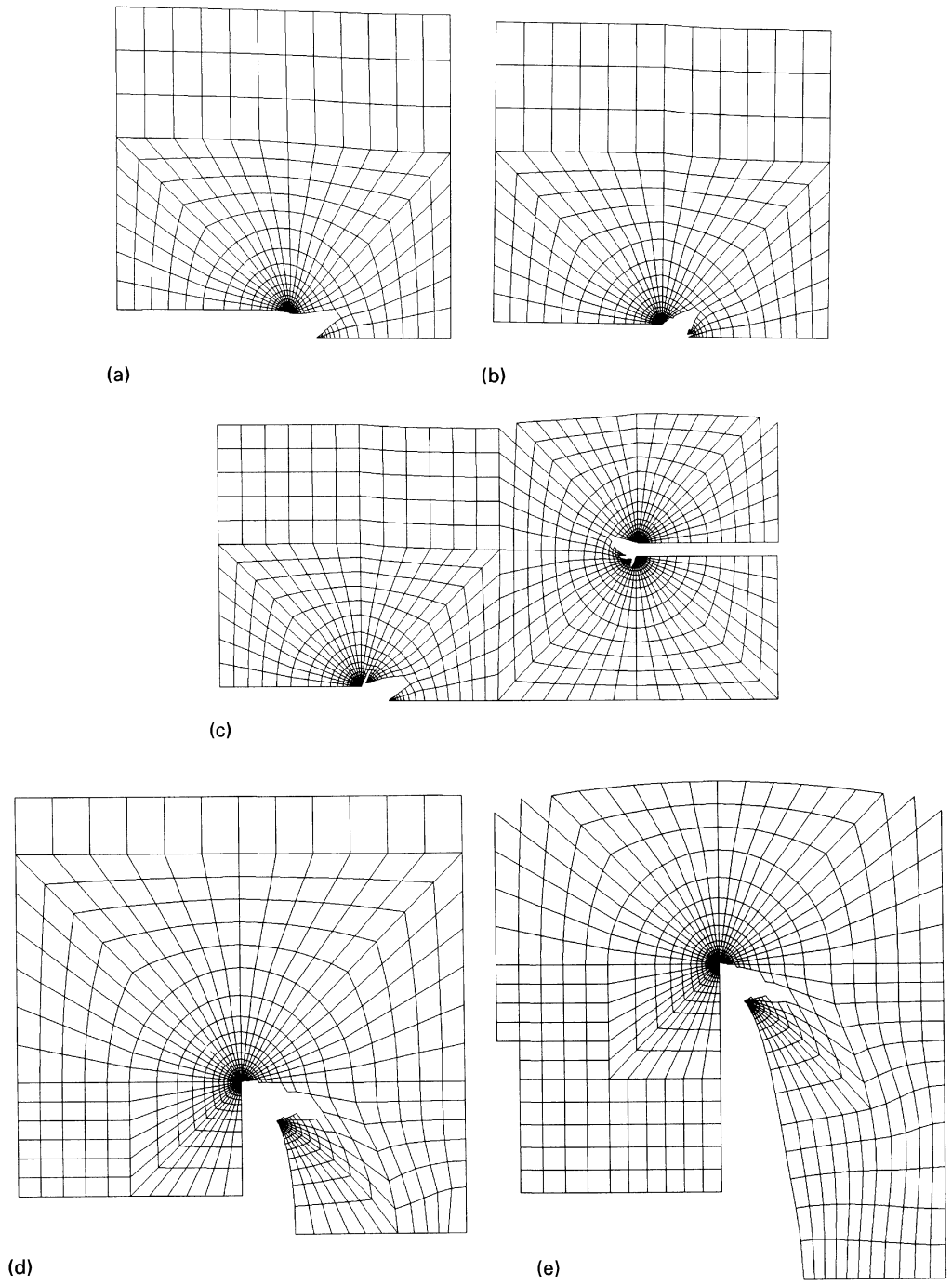

Figure 6 Comparison of the displacement fields near the crack tip and crack extensions at final load levels: (a) crack in the ductile layer as a homogenous isotropic case; (b) collinear cracks in the laminated composite; (c) multiple cracks in the laminated composite, (c) for a crack having a delamination with 0.1 times the original crack length in the laminated composite; (d) for a crack having a delamination with 0.2 times the original crack length in the laminated composite.

deformation zone for the delaminating cracks in the composite significantly differs from those seen previously and the formation of the very pronounced shear bands and the development of a large deformation zone at the centre of the uncracked ductile ligament, almost the deformation zone usually seen in the uniform tensile specimen, can be easily distinguished in Fig. 7d and e. Although it is not shown here as a separate figure, the distribution of the void volume fraction follows the distribution of the plastic strains since both the nucleation of the voids and their growth rate were assumed to be controlled by the plastic strains via Equations 5 and 6. It is apparent that, in the delaminated cracks, large-scale damage accumulation also occurs at the centre of the uncracked ductile ligament away from the current crack tip. For small delamination lengths the damage zone ahead of the crack tip and the damage zone occurring at the centre of the ductile ligament join very quickly, with the formation of the shear bands leading to significant drop both in the peak load and in the load-line displacement as seen in Fig. 3. With increasing delamination length, similar failure takes place; however, since the distance between these two damage zones is now

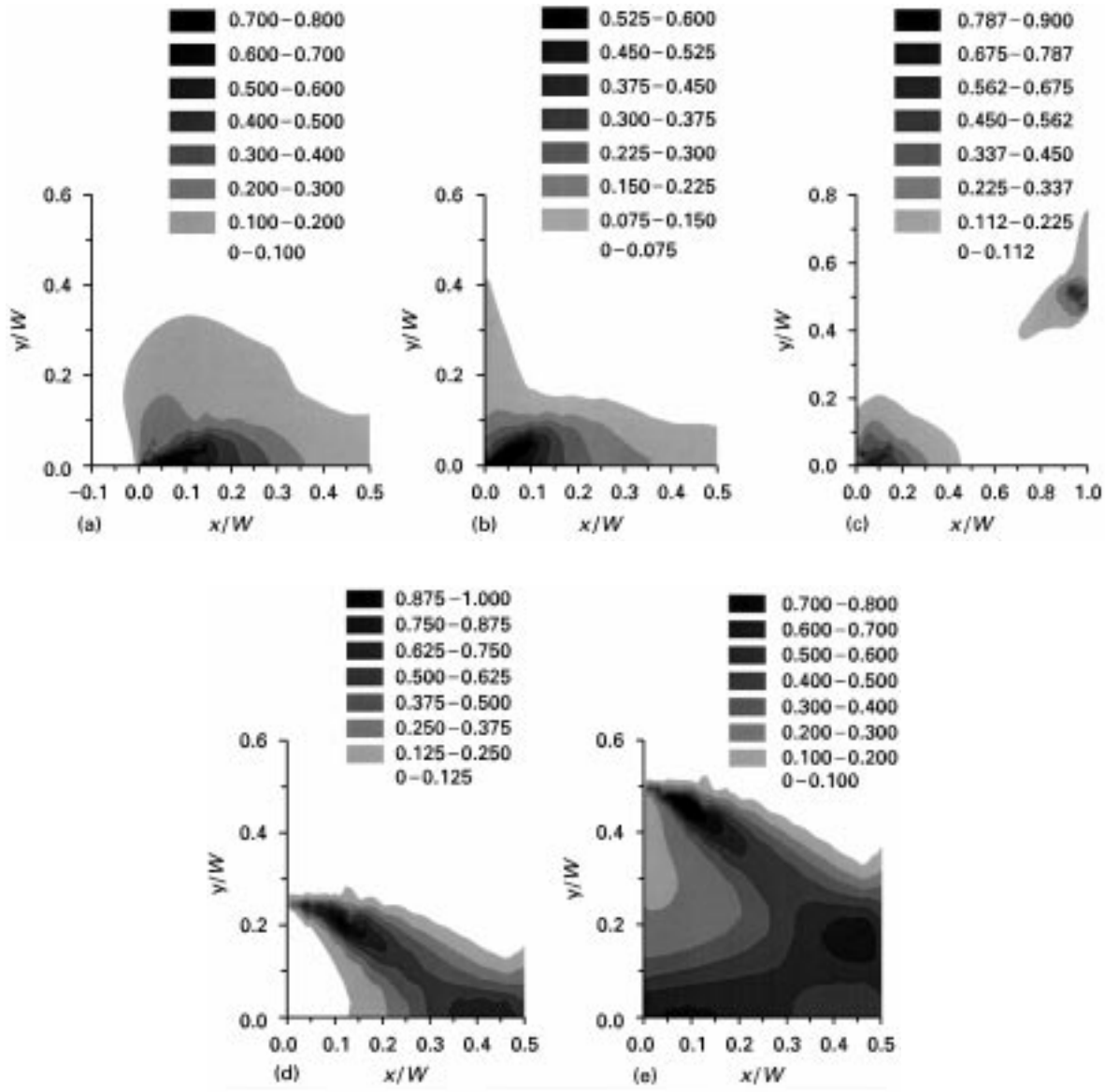

Figure 7 Comparison of the equivalent plastic strains at the final load levels: (a) crack in a ductile layer as a homogenous isotropic case; (b) collinear cracks in the laminated composite; (c) multiple cracks in the laminated composite; (c) for a crack having a delamination with 0.1 times the original crack length in the laminated composite; (d) for a crack having a delamination with 0.2 times the original crack length in the laminated composite.

increased and also the amount of material undergoing large-scale deformation is much larger (Figs 6e and 7e), the crack extension becomes more stable and requires much larger load-line displacements (Fig. 3).

The resulting R curves for the laminated composite having collinear cracks and cracks with delamination are compared with the R-curve behaviour of the crack in the ductile layer as a homogeneous isotropic case in Fig. 8. For the collinear cracks in the laminated composite in which the crack tip is located at the interface, in agreement with Fig. 4, the energy required for the initial crack extension into the ductile layer is much smaller than the energy required for the initial crack extension in the ductile layer as a homogeneous isotropic case. In the laminated composite, as the collinear cracks extend further into the ductile layer, the influence of the stress field of the interface region diminishes and the crack driving force becomes very similar to that seen for the crack in the ductile layer as a homogeneous isotropic case. Although R-curve behaviour is not shown for the multiple-crack case for clarity of the figure, the resulting R-curve behaviour was similar to that seen for the collinear crack case; this can also be inferred from Fig. 3. In the laminated composite having interface separation, fracture behaviour is very much dependent upon the delamination length. For short delamination lengths the energy required for crack initiation was similar to the collinear crack case; however, the energy required for crack extension in the ductile layer was much lower owing to the localization of deformation (Figs 6d and 7d). With increasing delamination length, the energy required for the crack initiation becomes similar to the crack in the ductile layer material, but further crack extension requires a much larger driving force owing to spread of the deformation into much larger regions and loss of stress triaxiality resulting from the development of a large zone in the centre of the uncracked ligament which has a significant amount of void formation (Figs 6e and 7e).

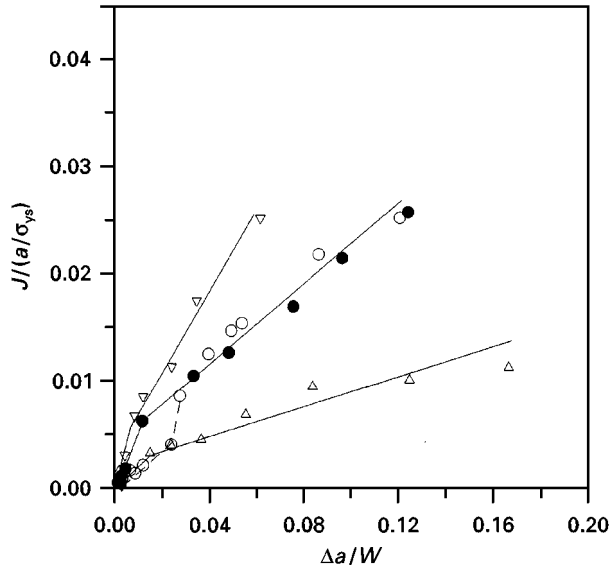

Figure 8 Crack resistance curves for collinear (○) and delaminating (interface crack I (△) and interface crack II (▽)) cracks in the laminated composite and comparison with the *R*-curve behaviour of the ductile layer material (●) as a homogenous isotropic case.

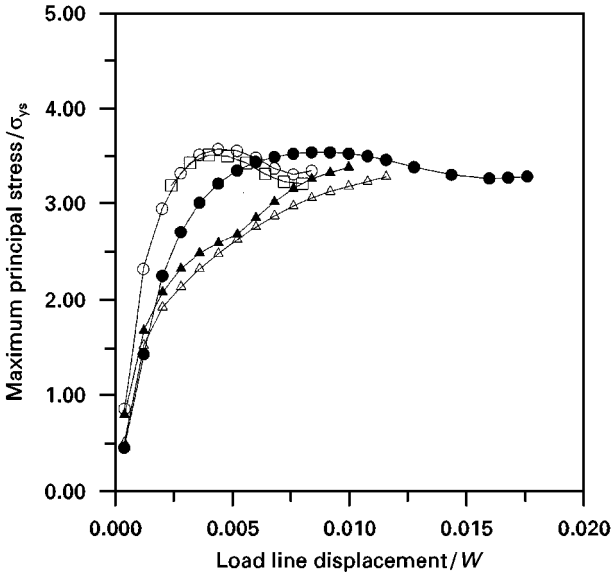

Figure 9 Variation in the maximum principal ahead of the crack tip at normalized distance, x/W, to the crack tip 2.3×10^{-3} before the first crack extensions. (○), composite with collinear cracks, (□), composite with multiple cracks; (△), composite with interface crack I; (▲), composite with interface crack II; (●), ductile layer.

For the cases investigated, the evolution of the maximum principal stress at the third ring elements up to first crack extension from the initial cracks are compared in Fig. 9. As can be seen, the elevation of the maximum principal stress for the collinear cracks and multiple cracks in the laminated composite occurs at a faster rate initially; with the extent of the plastic deformation and damage formation in the form of voids, the resulting maximum values becomes very similar to that seen for the crack in the ductile layer as a homogeneous isotropic case. In the case of the cracks having an interface separation, this build-up in the maximum principal stress occurs at a lower rate but also attains similar maximum values.

4. Discussion

The analyses presented in this study are not based on detailed quantitative data for the parameters that appear in the constitutive model of ductile layers of a particular laminated composite system. The residual stresses due to possible differences in the thermal expansion coefficients of the layers were also neglected during the analysis. Therefore, the results rather give mainly qualitative information about the influence of various crack geometries that are seen in the brittle layers of the laminated composites on the fracture behaviour of the ductile layers, and hence their contribution to the overall toughening characteristics in such composite systems.

For almost all the cases investigated, the initial damage accumulation in the form of nucleation and the growth of the voids in the ductile layers of the laminated composite has occurred much earlier than seen ahead of the crack in the ductile layer as a homogenous isotropic case (Figs 4 and 5). To elucidate this behaviour the angular distribution of the stress values in the absence of any void nucleation and growth, at the same angular distance where the void growth rates were reported earlier, are compared in Fig. 10. For the collinear cracks for which the crack tip was located at the interface, the occurrence of much larger axial and transverse stresses in comparison with the homogenous crack can be seen. Similarly, the occurrence of a much higher triaxial and equivalent stresses for the case of collinear cracks can also be discerned from the figure. Although the elevations of the transverse and axial stresses are lower, a larger shear stress develops in the case of the delaminating cracks than in both the other cases. The fast damage accumulation seen in Figs 4 and 5, and the resulting lower fracture energies required for the early crack extensions seen in Fig. 9 for the laminated composite are associated with this evolution of a higher stress state in the interface region. In the case of the collinear cracks, as the fracture progresses towards the centre of the ductile layer, the influence of the interface region diminishes and the energy required for the crack extension becomes similar to that seen for the crack in the ductile layer material as a homogenous isotropic case. It appears from Figs 3 and 6–8 that the ductile fracture behaviour of the ductile layers for the cracks having delamination is very much dependent upon the delamination length. For the small delamination lengths, the resulting *R*-curve behaviour is much lower than seen for the crack in the ductile layer material as a homogenous isotropic case owing to the formation of localized deformation. With increasing delamination length the ductile layers exhibit a higher resistance to fracture in the laminated composites resulting from spread of the deformation into much larger regions and owing to loss of stress triaxiality caused by the development of a large zone in the centre of the uncracked ligament which has a significant amount of void formation (Figs 6 and 7). This

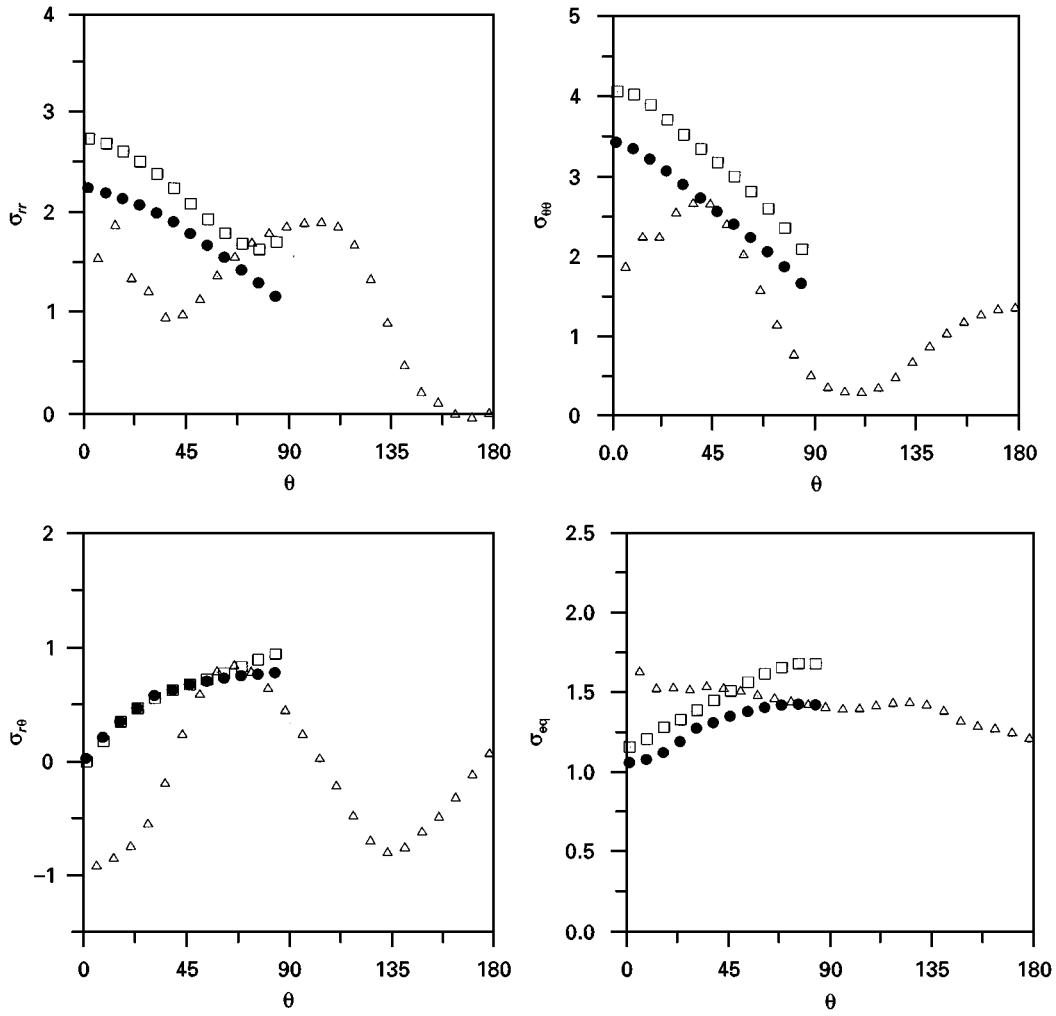

Figure 10 The angular stress distribution at a radial distance $2.3 \times 10^{-3} W$ ahead of the collinear and delaminating cracks in laminated composites in the absence of void nucleation and growth. (●), ductile reinforcement; (□), composite; (△), composite with interface II.

large-scale void formation in the central region of the ductile reinforcements also seen in many experimental studies [5, 12].

The ductile layer material exhibits a fracture mode associated with the nucleation and growth of voids as a homogenous isotropic material, in the laminated composite form; the change in the fracture mechanism of the ductile layers to cleavage or intergranular fracture modes has been observed in many composite systems reinforced with ductile layers having a b.c.c crystalline structure [1–9]. It is also now well established that, in order for brittle fracture (cleavage or intergranular) to take place, it is necessary not only that a critical fracture stress should be attained ahead of the crack tip but also that this stress level should be maintained for some microstructurally characteristic distance [26, 27]. When a comparison is made between Figs 9 and 10, although the initial stresses are much higher ahead of the cracks in the laminated composite, these high stresses relax very quickly before the first crack extension (Fig. 10), owing to faster evolution of void nucleation and growth (Figs 4 and 5), leading to attainment of the similar maximum principal stress level as seen for the crack in the ductile layer as a homogenous isotropic case (Fig. 9). On the basis of this observation, it should be expected that the same fracture mode will operate both in the composite form or as a homogenous material. To elucidate this behaviour further, in the next two simulations, for the collinear cracks, the crack tip location was moved from the interface into the brittle layer by an amount 0.034 times the original crack length. For these simulations it was assumed that the crack extension in the brittle layer occurs by attainment of a critical maximum principal stress, σ_f; its values were chosen as five and ten times the yield strength of the ductile layer. The resulting load–load-line displacement curve for $\sigma_f = 10\sigma_{ys}$ is compared with the previous cases in Fig. 11. As can be seen, after the large drop in the applied load as a result of the failure of the brittle ligament, the resulting load–load-line displacement curve is very similar to that seen for the collinear crack whose tip was previously located at the interface. Again the evolution of the maximum principal stress values for these cases, at the third ring elements up to formation of the first cracking in the ductile ligament due to nucleation and growth of voids, are shown in Fig. 12. As can be seen, the crack tip is now only 0.034 times the original crack length away from the interface of the brittle and ductile layer, the behaviour of the

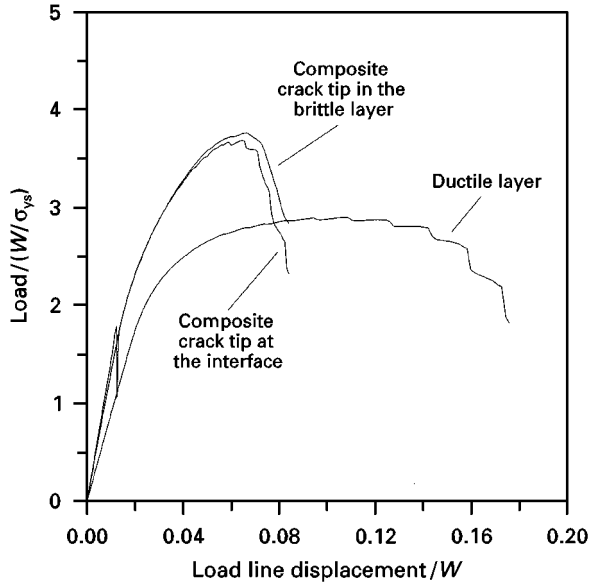

Figure 11 Load–load-line displacement responses of the composite having different collinear crack lengths.

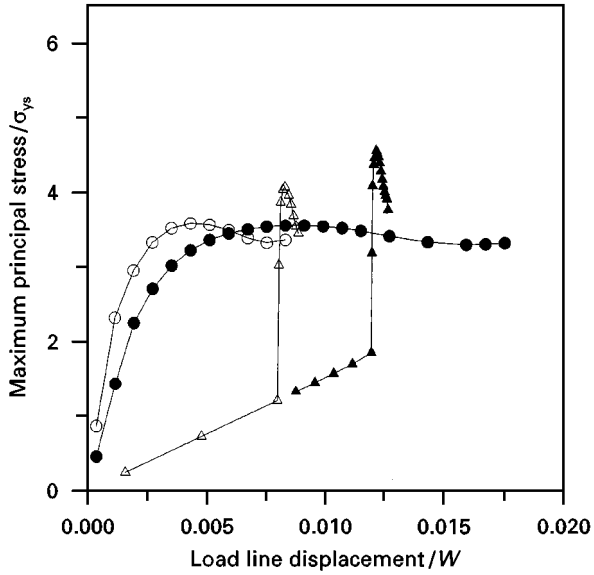

Figure 12 Variation in the maximum principal ahead of the crack tip at normalized distance, x/W, to the crack tip 2.3×10^{-3} before the first crack extensions for different collinear crack lengths and different failure strengths of the brittle layer. (○), composite crack as the interface; (Δ), composite crack in the brittle layer ($\sigma_f/\sigma_{ys} = S$); (▲), composite crack in the brittle layer ($\sigma_f/\sigma_{ys} = 10$); (●), ductile layer.

ductile layer is completely elastic and the maximum principal stress values increase linearly with increasing axial displacement. After the failure of the brittle ligament, the maximum stress levels attained are larger than those seen earlier and the magnitude increases with increasing σ_f/σ_{ys} ratio. These analyses were performed without any provision for the failure of the ductile layers with brittle fracture and only to indicate the possibility of larger evolution of maximum principal stress in the ductile layers; a much faster increase in the void volume fraction than seen in Fig. 4 causes very quick relaxation from the peak values with increasing deformation as seen in Fig. 12.

Although the results presented above are based on the continuum scale, they clearly indicate the role of the crack morphology (i.e., collinear versus multiple cracking), the extent of the delamination and crack tip location on the fracture behaviour of ductile layers and their possible contribution to overall composite toughening behaviour.

5. Conclusions

In this study the failure of the ductile layers in a laminated composite system was studied by using a constitutive relationship that accounts for strength degradation resulting from the nucleation and growth of voids. The results indicate the following.

1. In the laminated composites, the void nucleation and growth ahead of the cracks occur at a much faster rate owing to evolution of much higher stress values at the interface region.
2. Except for short crack extensions, collinear and multiple cracks develop similar crack resistance curves to that seen for a crack in the ductile layer material as a homogenous isotropic case.
3. For delaminating crack cases, the fracture behaviour is strongly influenced by the delamination length. The resistance of the ductile layers to the crack extension can be reduced significantly by short delamination lengths. For large delamination lengths the resistance to crack extension becomes greater than that seen for the ductile material.
4. Similar maximum stress values develop in the ductile layers as in the fracture test of the same ductile material if the crack tip is at the interface of the ductile and the brittle layers, suggesting that ductile–brittle fracture transition behaviour of the ductile layers is dependent upon the extent of the cracks in the brittle layers and fracture characteristics of the brittle layers.

Acknowledegements

This work was performed for the US Department of Energy by Iowa State University under Contract W-7405-Eng-82. This research was supported by the Director of Energy Research, Office of Basic Energy Sciences.

References

1. J. T. BEALS and V. C. NARDONE, *J. Mater. Sci.* **29** (1994) 2526.
2. L. SHAW and R. ABBASCHIAN, *Acta Metall. Mater.* **42** (1994) 213.
3. H. C. CAO, B. J. DALGLESIH, H. DAVE, C. ELLIOT, A. G. EVANS, R. MEHRABIAN and G. R. ODETTE, *ibid.* **38** (1990) 2969.
4. V. V. KRSTIC, P. S. NICHOLSON and R. G. HOAGLAND, *J. Amer. Ceram. Soc.* **64** (1981) 499.
5. J. KAJUCH, J. SHORT and J. J. LEWANDOWSKI, *Acta Metall. Mater.* **43** (1995) 1955.
6. L. XIAO and R. ABBASCHIAN, *Metall. Trans.* **24A** (1992) 403.
7. T. C. LU, A. G. EVANS, R. J. HECT and R. MEHRABIAN, *Acta Metall. Mater.* **39** (1991) 1853.

8. W. O. SOBOYEJO, F. YE, L.-C. CHEN, N. BAHTISHI, D. S. SCHWARTZ and R. J. LEDERICH, *Acta Mater.* **44** (1996) 2027.
9. J. KAJUCH, J. D. RIGNEY and J. J. LEWANDOWSKI, *Mater. Sci. Engng* **A115** (1992) 59.
10. C. K. SYN, S. STONER, D. R. LESUER and O. D. SHERBY, in "High performance metal and ceramic composites", edited by K. Upadhya (Metallurgical society of AIME, Warrendale, PA, 1994) p. 125.
11. W. H. HUNT Jr, T. M. OSMAN and J. J. LEWANDOWSKI, *J. Metals* **45** (1993) 30.
12. M. BANNISTER, H. SHERCLIFF, G. BAO, F. ZOK and M. F. ASHBY, *Acta Metall. Mater.* **40** (1992) 1531.
13. A. G. EVANS and R. McMEEKING, *Acta Metall. Mater.* **34** (1986) 241.
14. S. B. BINER, *Mater. Sci. Engng.* **A187** (1994) 125.
15. RAVICHANDRAN, *Acta Metall. Mater.* **40** (1992) 1009.
16. BUDINASKY, J. C. AMAZIGO and A. G. EVANS, *J. Mech. Phys. Solids* **36** (1988) 167.
17. F. ERDOGAN and P. F. JOSEPH, *J. Amer. Ceram. Soc.* **72** (1989) 262.
18. A. L. GURSON, PhD thesis, Brown University (1975).
19. *Idem.*, *J. Eng. Mater. Technol.* **99** (1977) 2.
20. V. TVERGAARD, *Int. J. Fract.* **17** (1981) 389.
21. *Idem.*, *ibid.* **18** (1982) 237.
22. V. TVERGAARD and A. NEEDLEMAN, *Acta Metall. Mater.* **32** (1988) 157.
23. C. C. CHU and A. NEEDLEMAN, *J. Engng Mater. Technol.* **102** (1980) 249.
24. V. TVERGAARD, *Acta Metall. Mater.* **38** (1990) 185.
25. B. MORAN and C. F. SHIH, *Engng Fract. Mech.* **27** (1987) 615.
26. R. O. RITCHIE, J. F. KNOTT and J. R. RICE, *J. Mech. Phys. Solids* **21** (1973) 395.
27. A. W. THOMPSON and J. F. KNOTT, *Metall. Trans.* **A24** (1993) 523.

Received 16 April 1997
and accepted 2 April 1998